ELSEVIER

Applied Surface Science 127–129 (1998) 947–952

applied surface science

# Electron beam ablation versus laser ablation: plasma plume diagnostic studies

S.D. Kovaleski, R.M. Gilgenbach *, L.K. Ang, Y.Y. Lau, J.S. Lash [1]

*Intense Energy Beam Interaction Laboratory, Nuclear Engineering and Radiological Sciences Department, University of Michigan, Ann Arbor, MI 48109-2104, USA*

**Abstract**

Experiments have been performed to compare XeCl laser ablation plume characteristics to those produced by electron beam ablation. Potential advantages of electron beams include higher electrical efficiency ($\sim 30\%$), and the ability to process materials with high optical reflectivity or transparency. The electron beam is generated by a channelspark with parameters: peak voltage of 15–20 kV, current of 1.5–1.7 kA, and pulse length of about 200 ns. The electron beam is ion focused to about 2 mm diameter by an argon background gas. Initial diagnostic experiments have utilized optical emission spectroscopy to characterize the ionization dynamics of the ablation plumes of Fe targets. Spectra taken during electron beam ablation are composed of singly ionized iron, with negligible emission from neutral iron. This is in sharp contrast with XeCl excimer laser ablation, which is composed of both neutral and ion species, the neutrals persisting strongly after the laser pulse. In addition to Fe ion emission, the channelspark emission spectrum also exhibits a high degree of excitation and ionization of the Ar background gas. Strong emission from $Ar^{+}$, $Ar^{2+}$, and $Ar^{3+}$ has been measured. © 1998 Elsevier Science B.V.

*PACS:* 52.40.− w; 52.75.Rx; 61.80.− x; 61.80.Ba

*Keywords:* Electron beam; Electron beam ablation; Channelspark; Ablation plasma; Plasma spectroscopy

## 1. Introduction

Pulsed ablative deposition has proven to be an important new process for thin films of hard-to-deposit materials, such as cubic BN [1] and diamond-like carbon [2]. Excimer lasers (KrF or XeCl) have typically been utilized for ablative deposition. Advantages of laser ablation include preservation of stoichiometry of compounds (e.g., $YBa_2Cu_3O_{7-x}$) [3] and generation of high energy ions which promote film growth [1]. Low current electron beams have been employed by Dickinson et al. [4] to enhance laser absorption by generation of defects in insulators.

However, within the past several years, advances have been made in the technology of high current (kA), moderate voltage (15–20 kV), channelspark electron beams [5,6]. The incident peak power density ($\sim 10^9$ W/cm$^2$) and incident fluence (10–30 J/cm$^2$) of these channelspark electron beams are

* Corresponding author. University of Michigan, RM 1906, Cooley Bldg., 2355 Bonisteel Ave., Ann Arbor, MI 48109, USA. Tel.: +1-734-763-1261; fax: +1-734-763-4540; e-mail: rongilg@engin.umich.edu.

[1] Now at Sandia National Laboratory.


*PII* S0169-4332(97)00771-X

Table 1
A comparative list of important XeCl and channelspark parameters for Fe targets

| Parameter | Channelspark | XeCl excimer laser |
|---|---|---|
| Energy deposited (J) | $< 1$ | $< 0.05$ |
| Peak Power (MW) | $< 15$ | 2.5 |
| Fluence ($J/cm^2$) | $< 30$ | $< 13$ |
| Power density ($MW/cm^2$) | $< 500$ | 600 |
| Energy density ($MJ/cm^3$) | $< 0.5$ | 3 |
| Spot size ($cm^2$) | 0.03 | 0.004 |
| Energy deposition depth ($\mu$m) | 0.6 | 0.04 |
| Pulselength (ns) | 200 | 40 |
| Accelerating potential (kV) | 15–20 | – |
| Beam current (A) | $\sim 1500$ | – |
| Background gas pressure (mTorr) | $\sim 12.5$ (necessary) | $\sim 12.5$ (not necessary) |

comparable to that of typical excimer lasers, as listed in Table 1. The key feature of the moderate energy electron beam is the short electron range (typically $\sim \mu$m in metals), which deposits the e-beam energy near the surface of the material. Electron beam ablation has a number of potential advantages: (1) High electrical efficiency (typically about 30%), (2) low reflected e-beam energy fraction for materials which are transparent (e.g., fused silica) or highly reflective (e.g., Al) of laser light, (3) electron beam promotes dissociation, excitation, and ionization of fill gas (which could be important for deposition of metal nitrides like BN and TiN in nitrogen gas), and (4) environmentally attractive since no toxic gases are required.

In order to evaluate the relative merits of electron beam ablation vs. laser ablation, we present here a diagnostic study of the ablated plasma plumes. Of particular interest in the present study are the ionization dynamics of both the ablated plume and the Ar fill gas.

## 2. Experimental configuration

Fig. 1 shows the combined experimental configuration for channelspark electron beam ablation and XeCl excimer laser ablation. This channelspark was procured from Kernforschungszentrum Karlsruhe [5]. The experiments were performed in stainless steel vacuum crosses evacuated with a turbomolecular pump. For both sources, the chamber was backfilled with about 12 mTorr of Ar gas; the optimal pressure for channelspark electron beam generation and propagation. In either case, the target was an iron foil, 0.25 mm thick and 99.99% pure.

The channelspark electron beam is transported to the target through an 8 cm long alumina beam guide tube, with outer and inner diameters of 7 mm and 3 mm, respectively. The target was positioned 1 cm from the end of the beam guide tube, and was angled 45° from the line of e-beam propagation (Fig. 2). The channelspark e-beam target current (typically 1500–1700 A) was measured with a Pearson current transformer (Fig. 1). Many target current traces had a microsecond plasma current tail, believed due to $L/R$ decay of the plasma current. The channelspark charging voltage was usually around 18 kV.

Laser ablation plumes were generated by focusing a Lambda-Physik LPX105 MC XeCl excimer laser ($\sim 50$ mJ, 40 ns, 308 nm) with a $f = 250$ mm lens onto a 0.004 $cm^2$ spot at the target. A PIN diode-measured temporal pulse shape is shown in Fig. 1. Typical laser parameters are shown, and compared to typical channelspark e-beam parameters in Table 1.

Optical emission spectroscopy was performed with a 0.300 m Acton 300i imaging spectrograph utilizing a 2400 lines/mm grating blazed at 240 nm, with an attached Princeton Instruments ICCD-576/RB-EM intensified, gated CCD detector ($576 \times 384$ pixels). Wavelength calibration of the spectrograph was performed using an Oriel Hg (Ar) spectral calibration lamp. The camera was externally gated with adjustable gates and delays on nanosecond time scales.

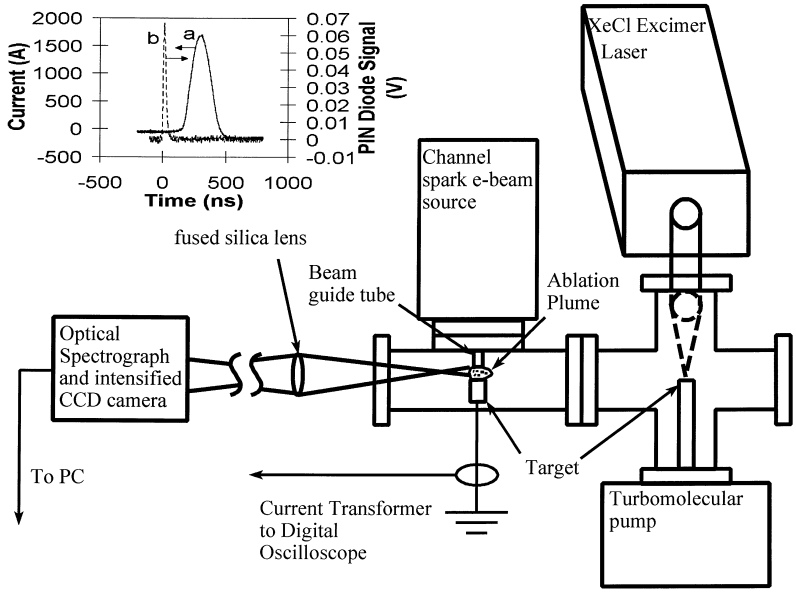


Fig. 1. Combined experimental configuration for channelspark and XeCl excimer laser ablation, including temporal pulse shapes. Inset: (a) Channelspark electron beam target current, for a low pressure case, (b) PIN diode measurement of the XeCl laser pulse.

The channelspark and XeCl ablation plumes were imaged on the slit of the spectrograph with fused silica lenses of $f = 250$ mm and $f = 360$ mm, respectively. A 20 $\mu$m slit was used, positioned about 1 mm from the target and parallel to the target surface for excimer laser ablation. Due to the necessity of angling the target in e-beam ablation, the slit was positioned 45° relative to the target surface (parallel to the e-beam) and crossing the surface such that the center of the slit was about 1 mm from the beam impact point.

## 3. Results and discussion

Fig. 2 shows a time integrated open shutter picture (Polaroid 667 film) of e-beam ablation. A schematic explains the features of the photo, which apparently shows strong light emission from the e-beam interaction with the argon fill gas, as well as plume light perpendicular to the target surface.

Figs. 3 and 4 show an example of optical emission spectra of channelspark electron beam ablation vs. laser ablation of Fe. The wavelength range chosen for Figs. 3 and 4 encompasses both strong neutral and singly ionized Fe lines, as well as several $Ar^{3+}$ and one $Ar^{2+}$ emission lines. All line assignments used throughout this paper were taken from the NIST database for atomic spectroscopy [7]. A notable difference between these two spectra is the presence of neutral Fe emission in the excimer laser ablation case, and the lack thereof in the channelspark case. This can be explained by the presence of energetic electrons ($< 15$ keV) for plume ionization in electron beam ablation. Moderate energy electrons are also reflected from the target (estimated at $\sim 20\%$ reflected fraction by Sandia's TIGER code) [8]. Additionally, low energy electrons are liberated as the beam ionizes the Ar fill gas to form the positively charged ion focusing channel; these are energetically expelled by the space charge of the electron beam itself [9]. The ionization of the e-beam ablation plume is so strong that negligible neutral Fe emission is measured during or after the e-beam pulse. For the e-beam case, Fig. 3 also exhibits several $Ar^{3+}$ and one $Ar^{2+}$ line. Other parts of the spectrum also have shown very strong emission from $Ar^{+}$ with little emission from neutral Ar. The high degree of ionization and excitation of the background gas by the e-beam could prove useful in the deposition of metal nitrides in nitrogen backgrounds

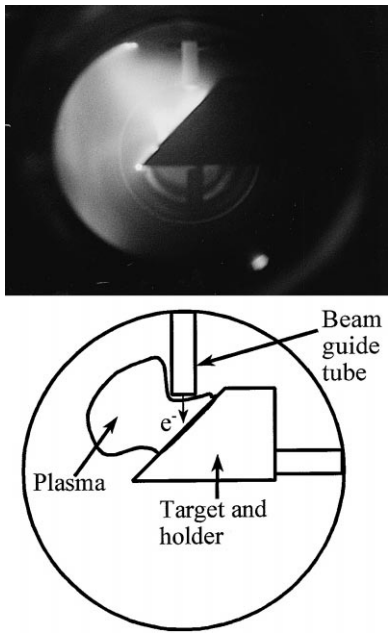


Fig. 2. Open shutter picture, integrating the optical emission from the entire ablation pulse, of channelspark ablation. Also included is a schematic pointing out the various features of the photograph.

[10]. By contrast, the XeCl laser ablation showed negligible emission from the argon fill gas.

Temporal resolution of the optical emission of e-beam and laser generated plasmas was accomplished by gating the intensified CCD camera in 100

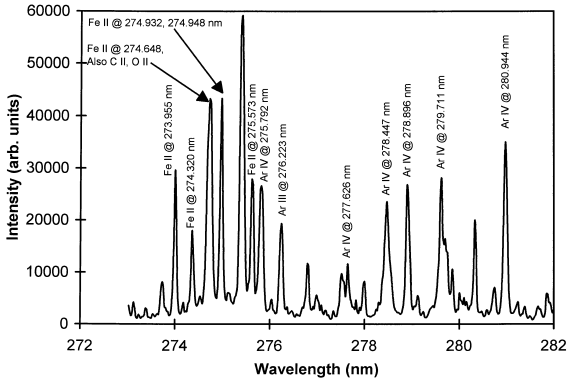


Fig. 3. Optical emission spectrum from channelspark ablation of Fe in 12.5 mTorr of Ar gas. Light is collected during gate pulse of 150 ns to 250 ns, measured relative to 10% of maximum current on the initial current rise. (Line at 275.4 nm is unidentified and could be due to contaminants.)

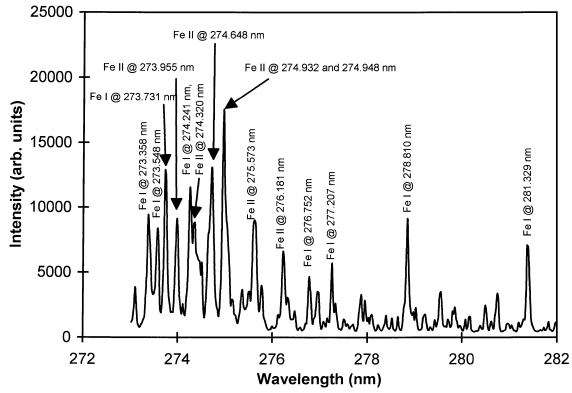


Fig. 4. Optical emission spectrum from XeCl excimer laser ablation of Fe in 11.4 mTorr of Ar gas. Light is collected during gate pulse of 180 ns to 280 ns after the laser pulse.

ns gates for the channelspark and 100 ns and 50 ns gates for the XeCl laser. The gates were then delayed through the duration and after the e-beam and laser pulses. Fig. 5 shows the emission intensity, during channelspark ablation, of four $Fe^{+}$ lines at 273.955 nm, 274.932 and 274.948 nm, and 275.573 nm during 100 ns gates, delayed in 100 ns intervals during and after the pulse. The times at which the intensities are plotted correspond to the center of the 100 ns gate and were measured relative to the initial 10% of

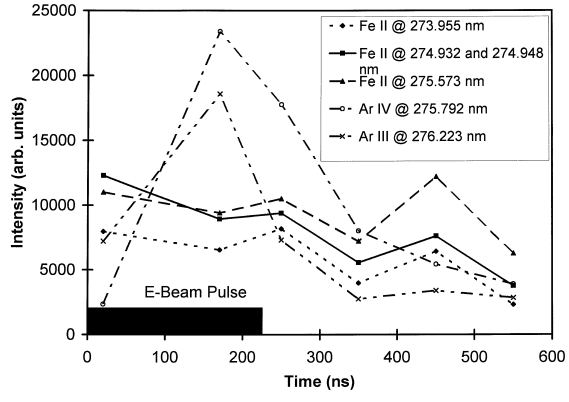


Fig. 5. Plot of the optical emission intensity of several Fe(II), Ar(III), and Ar(IV) lines present in the spectrum of channelspark ablation plasmas with respect to time. Each intensity is the result of three averaged gate widths, 100 ns long, centered at the times at which a point is plotted. All times are measured relative to 10% of the maximum current in the initial current rise. Lines are a guide for the eye.

peak e-beam current during the current rise. Also shown are the intensities of an $Ar^{2+}$ line at 276.223 nm and $Ar^{3+}$ at 275.792 nm. The intensities measured are uncorrected for instrument response, but have been collected within a narrow wavelength range. For the first three 100 ns gates, centered at 20 ns, 170 ns, and 250 ns respectively, the $Fe^{+}$ emission is large, between 7000 and 13 000 counts. By the fourth gate, centered at 350 ns, singly ionized iron emission is beginning to fall off, but remains above 2000 counts. After the e-beam pulse has passed, in late time, the channelspark plasma begins to become unstable due to unipolar arcing at the target [11]. This can lead to a significant amount of fluctuation in $Fe^{+}$ emission for late time data collection. $Ar^{2+}$ and $Ar^{3+}$ emissions rise quickly between the first gate, centered at 20 ns, and the second centered at 170 ns; they then fall in the next gate centered at 250 ns, and fall off quickly after the e-beam pulse has passed. This shows that the Ar ion emission tracks the channelspark electron beam current very closely.

Fig. 6 shows the emission intensity of neutral Fe and singly ionized Fe for XeCl excimer laser ablation. The intensities plotted to the left of the vertical dotted line in Fig. 6 are an average of three 50 ns gates taken with the same delays (with the exception of the gate centered at 235 ns, which is an average of only two gates), measured relative to the beginning of the laser pulse. The intensities plotted to the right of the vertical dotted line are an average of three 100 ns gates taken with the same delays also measured relative to the beginning of the laser pulse. The times at which these intensities are plotted correspond to the centers of the 50 and 100 ns gates. The same $Fe^{+}$ lines are presented here as in Fig. 5. For the first 50 ns gate centered at 35 ns, the $Fe^{+}$ emission is at its highest, around 40 000 counts. By the second gate, centered at 85 ns, the $Fe^{+}$ emission has fallen to about 28 000 counts and by the fifth and sixth gates, centered at 235 ns and 285 ns, respectively to less than 2000 counts. Also plotted in this figure are two Fe neutral lines. These lines are also at their maximum at more than 7000 counts during the first gate, but fall less quickly than the $Fe^{+}$ lines, to about the same intensity by the sixth gate at 285 ns. In the late time, 100 ns gates, starting with the seventh gate centered at 360 ns, the Fe neutral emissions have surpassed the $Fe^{+}$ emission intensities, most likely as a result of recombination. This is in sharp contrast to e-beam ablation, where negligible neutral Fe emission is measured on these timescales.

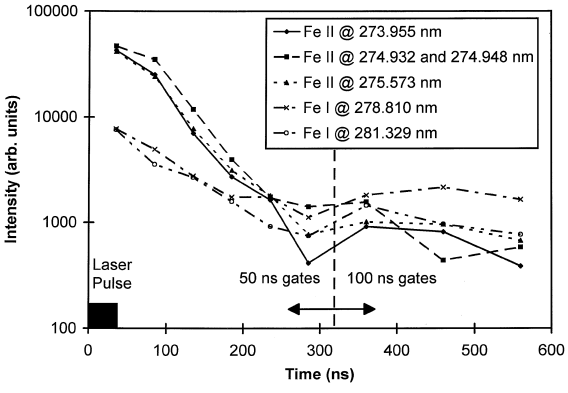


Fig. 6. Plot of the optical emission intensity of several Fe(I) and Fe(II) lines present in the spectrum of XeCl excimer laser ablation plasmas with respect to time. Each intensity is the result of three averaged gate widths, 50 ns long to the left of the vertical dotted line and 100 ns long to the right of the vertical dotted line, centered at the times at which a point is plotted. All times are measured relative to the rise of the laser pulse. Intensities are plotted on a logarithmic scale to better present late time data. Lines are a guide for the eye.

## Acknowledgements

This research was supported by National Science Foundation Grant CTS-9522282. Equipment donations from General Motors Research and Development Center are appreciated.

## References

[1] G.L. Doll, J.A. Sell, C.A. Taylor, R. Clarke, Phys. Rev. B 43 (1991) 6816.
[2] A.A. Voevodin, M.A. Capano, A.J. Safriet, M.S. Donley, J.S. Zabinski, Appl. Phys. Lett. 69 (1996) 188.
[3] S.R. Foltyn, P. Tiwari, R.C. Dye, M.Q. Le, X.D. Wu, Appl. Phys. Lett. 63 (1993) 1848.
[4] J.T. Dickinson, S.C. Langford, L.C. Jensen, P.A. Eschbach, J. Appl. Phys. 68 (1990) 1831.

[5] G. Muller, C. Schultheiss, Proc. of Beams '94, San Diego, CA 2 (1994) 833.
[6] Q.D. Jiang, F.C. Matacotta, M. Konijnenberg, G. Muller, C. Schultheiss, Thin Solid Films 241 (1994) 100.
[7] J. Reader, C.H. Corliss (Eds.), NIST Spectroscopic Properties of Atoms and Atomic Ions Database, US Secretary of Commerce, 1992.
[8] Sandia Report No. SAND 91-1634.
[9] J.D. Miller, R.M. Gilgenbach, IEEE Trans. Plasma Sci. 18 (1990) 658.
[10] M.G. Norton, P.G. Kotula, C.B. Carter, J. Appl. Phys. 70 (1991) 2871.
[11] Th. Witke, A. Lenk, B. Shultrich, C. Schultheiss, Surf. Coat. Technol. 74–75 (1995) 580.